

1 **Mapping global forest age from forest inventories, biomass and climate data**

2 Simon Besnard^{1,2}, Sujan Koirala¹, Maurizio Santoro⁵, Ulrich Weber¹, Jacob Nelson¹, Jonas Gütter^{1,4},
3 Bruno Herault^{6,7}, Justin Kassi⁸, Anny N'Guessan⁸, Christopher Neigh⁹, Benjamin Poulter⁹, Tao
4 Zhang^{10,11}, Nuno Carvalhais^{1,3}

5

6 ¹Max Planck Institute for Biogeochemistry, Germany

7 ²Laboratory of Geo-Information Science and Remote Sensing, Wageningen University & Research, The Netherlands

8 ³Departamento de Ciências e Engenharia do Ambiente, DCEA, Faculdade de Ciências e Tecnologia, FCT, Universidade
9 Nova de Lisboa, Portugal

10 ⁴DLR, Institute of Data Science Data Management and Analysis, Germany

11 ⁵Gamma Remote Sensing, Switzerland

12 ⁶INP-HB, Institut National Polytechnique Félix Houphouët-Boigny, Côte d'Ivoire

13 ⁷Cirad, University of Montpellier, UR Forests & Societies, France

14 ⁸Université Félix Houphouët-Boigny, UFR Biosciences, Laboratoire de Botanique, Côte d'Ivoire

15 ⁹NASA Goddard Space Flight Center, Biospheric Sciences Lab., Greenbelt, MD, USA

16 ¹⁰University of Florida, Department of Biology, United States

17 ¹¹University of Minnesota, Department of Forest Resources, United States

18

19 *Correspondence to:* Simon Besnard (sbesnard@bgc-jena.mpg.de) and Nuno Carvalhais (ncarvalhais@bgc-jena.mpg.de)

20 **Abstract.** Forest age can determine the capacity of a forest to uptake carbon from the atmosphere. Yet, a lack of global
21 diagnostics that reflect the forest stage and associated disturbance regimes hampers the quantification of age-related
22 differences in forest carbon dynamics. ~~In this study, we provide~~ a new global distribution of forest age circa 2010,
23 estimated using a machine learning approach trained with more than 40,000 plots using forest inventory, biomass and
24 climate data. First, ~~an evaluation against the plot level forest age measurements of forest age~~ reveals that the data-driven
25 method has a relatively good predictive capacity of classifying old-growth vs. non-old-growth (precision = 0.81 and
26 0.99 for old-growth and non-old-growth, respectively) forests and estimating corresponding forest ages (NSE = 0.6 and
27 RMSE = 50 years). ~~Yet~~ **However**, there are systematic biases with overestimation in young and underestimation in old
28 forest stands, respectively. Globally, we find a large variability of forest age with the old-growth forests in the tropical
29 regions of Amazon and Congo, ~~and~~ young forests in China and intermediate stands in Europe. ~~On the other~~
30 ~~hand~~ **Furthermore**, we find that the regions with high rates of deforestation or forest degradation (e.g., the arc of
31 deforestation in the Amazon) are ~~largely~~ composed ~~mainly~~ of younger stands. Assessment of forest age in the climate-
32 space shows that the old-forests are either in cold and dry regions or in warm and wet regions, while young-
33 intermediate forests span a large climatic gradient. Finally, a comparison between the presented forest age estimates
34 with a series of regional products reveals differences rooted in different approaches ~~as well as~~ ~~and~~ in different in-situ
35 observations and global-scale products. Despite showing robustness in cross-validation results, additional
36 methodological insights on further developments should as much as possible harmonize data across the different
37 approaches. The forest age dataset presented here provides additional insights into the global distribution of forest age
38 ~~in support of a~~ better understanding of the global dynamics in the forest water and carbon cycles. The forest age
39 datasets are openly available at <https://doi.org/10.17871/ForestAgeBGI.2021> (Besnard et al., 2021). ~~For anonymous~~
40 ~~access during review, please refer to the data availability section below.~~

41 **1 Introduction**

42 Forests cover about 30% of the terrestrial surface of our planet and store a large part of the terrestrial carbon, indicating
43 their fundamental role in the terrestrial carbon cycle (Bar-On, Phillips, and Milo, 2018). ~~Yet~~ **However**, drivers
44 controlling the capacity of the terrestrial biosphere to sequester carbon remain poorly characterized, limiting our
45 understanding of the global land carbon sink's location (Cook-Patton et al., 2020). Such uncertainties on the
46 geographical distribution of the carbon sink have been partly attributed to the fact that forest regrowth and demography
47 are not systematically considered for understanding changes in the forest carbon sink (Pugh et al., 2019, Zscheischler et
48 al., 2017).

49 While the recent increase in the forest carbon sink is controlled by environmental changes such as carbon dioxide (CO₂)
50 fertilization, nitrogen deposition, and climate change (Zhu et al., 2016), the dynamics in the forest carbon balance are
51 also attributed to disturbance history and forest regrowth (Pugh et al., 2019; Besnard et al. 2019; Amiro et al., 2010).
52 Forest disturbances cause physical damages to vegetation properties and changes in forest demography, thereby
53 affecting the balance of terrestrial CO₂ exchange with the atmosphere by temporarily increasing respiration and
54 reducing photosynthesis (Birdsey et al., 2006; Johnson and Curtis, 2001; Liu et al., 2011; Schimel, 2007; Williams et
55 al., 2012; Woodbury et al., 2007). The changes in the strength of carbon uptake or release can alter the forest carbon
56 balance by converting forest ecosystems from carbon sinks to sources (Amiro et al., 2010; Bowman et al., 2009; Ciais et
57 al., 2014; Moore et al., 2013). Odum (1969) hypothesized the first theory to describe the ecosystem development in the
58 absence of ~~major~~ **significant** disturbance, suggesting that the age of forests and ~~how~~ demographic changes drive carbon

59 accumulation. ~~Yet~~Nevertheless, an intrinsic property of a stand age distribution can be modified to varying degrees of
60 changes in environmental conditions and disturbance, therefore slowly change along with a foreststand age or
61 successional continuum (Irvine et al., 2005; Piloniot et al., 2018).

62 Despite the sensitivity of the forest carbon balance to disturbance and regrowth (Buitenwerf et al., 2018; Sulla-Menashe
63 et al., 2018), existing empirical models and current bottom-up spatiotemporal assessment of CO₂ fluxes do not
64 explicitly account for these effects (Jung et al., 2020; Tramontana et al., 2016; Jung et al., 2011). By not explicitly
65 constraining data-driven statistical models with disturbance history or forest demography, the forest carbon balance in
66 regions with newly disturbed forests and old-growth forests may not be realistically estimated. For instance, large
67 discrepancies are observed between bottom-up statistical ~~bottom-up~~ approaches (e.g., FLUXCOM initiatives,
68 <http://www.fluxcom.org/>) and atmospheric inversions in estimating net ecosystem exchange (NEE), particularly in the
69 tropics where site history plays a substantial role in NEE magnitude (Pugh et al., 2019). To account for the contribution
70 of disturbance on the land carbon sink, we need information on the geographical distribution of disturbance ~~is therefore~~
71 required, albeit such information is rathersomewhat limited at the global scale (Ciais et al., 2014). Forest age, related to
72 time since disturbance, can be seen as a useful surrogate in analyses of the impact of disturbance on the ability of forests
73 to sequester and store carbon. Incorporating forest age into terrestrial biosphere modelling offers a starting point to
74 characterize disturbance history, ~~therefore to so~~ getting more insights ~~on into~~ the location of the terrestrial carbon sinks
75 (Pugh et al., 2019). Reliable estimates of gridded forest age are, therefore, an importantessential and needed source of
76 information. The recent advances in describing the geographical distribution of forest demography globally (Huang et
77 al., 2010; Kennedy et al., 2010; Poulter et al., 2019) have paved the way to consider forest age and disturbance history
78 in carbon cycle studies.

79 Here, we aim to provide a new gridded global forest age dataset *circa* 2010 inferred from a compilation of forest
80 inventory, biomass and climate data. More specifically, we introduce the *in-situ* forest inventory dataset and the
81 modelling framework used in this study, as well as the predictive capacity of the presented model to infer forest age at
82 the plot level. We further describe the global and regional patterns of the gridded forest age dataset and their
83 uncertainties. The presented forest age dataset is finally benchmarked against a series of independent regional and
84 global datasets.

85 **2 Method**

86 **2.1 Forest inventory and climate data**

87 The globally gridded forest age dataset was developed by collecting *in-situ* plot level stand age, and aboveground
88 biomass (AGB) estimates from a series of forest inventory databases (Álvarez-Dávila et al., 2017; Anderson-Teixeira et
89 al., 2018; Anderson-Teixeira et al., 2016; Baker et al., 2016; Johnson et al., 2016; Lewis et al., 2013; Mitchard et al.,
90 2014; N'Guessan et al., 2019; Poorter et al., 2016; Schepaschenko et al., 2017; Somogyi et al., 2008; Sullivan et al.,
91 2017). Besides, we sampled 20,000 observations from the US Forest Service Forest Inventory and Analysis (FIA) data
92 (Burill et al. 2018) containing *in-situ* plot level stand age and aboveground biomass (AGB) estimates (the original
93 number of observations in the FIA dataset = 350,000). To reduce the unbalanced sample size across age classes, we
94 weight-sampled the FIA data with decadal age classes ~~that are~~ underrepresented in the dataset before including the FIA
95 data having higher weights. The weights for each decadal class were calculated following Eq. (1):

$$96 \text{ weight}_i = \frac{1}{n} \sum_{i=1}^n N \text{ age class}_i \quad (1)$$

97 | Where i is a decadal class and N_i is the number of observations.

98 | The methods used in inventory surveys to estimate stand age relied on expert knowledge, tree diameter measurements,
99 | tree rings from cores of selected trees (e.g., Burill et al. 2018), and/or semi-directive interviews (e.g., N’Guessan et al.,
100 | 2019). Forest inventory plots were classified as old-growth forests when stand age was more than or equal to 300 years.
101 | In total, the final dataset had around 25,000 plots and around 44,000 observations. Geographical biases were observed
102 | in the compiled dataset (Fig. 1), with North America, Europe and South East of China being well represented, while
103 | Africa, Indonesia, and Australia being either underrepresented or not represented at all. The Amazon basin and the
104 | West part of Eurasia were relatively well represented. Besides, stand age data were generally collected in locations
105 | easily accessible; therefore unmanaged forests in remote areas were very likely less represented than managed forests.

106

107

108

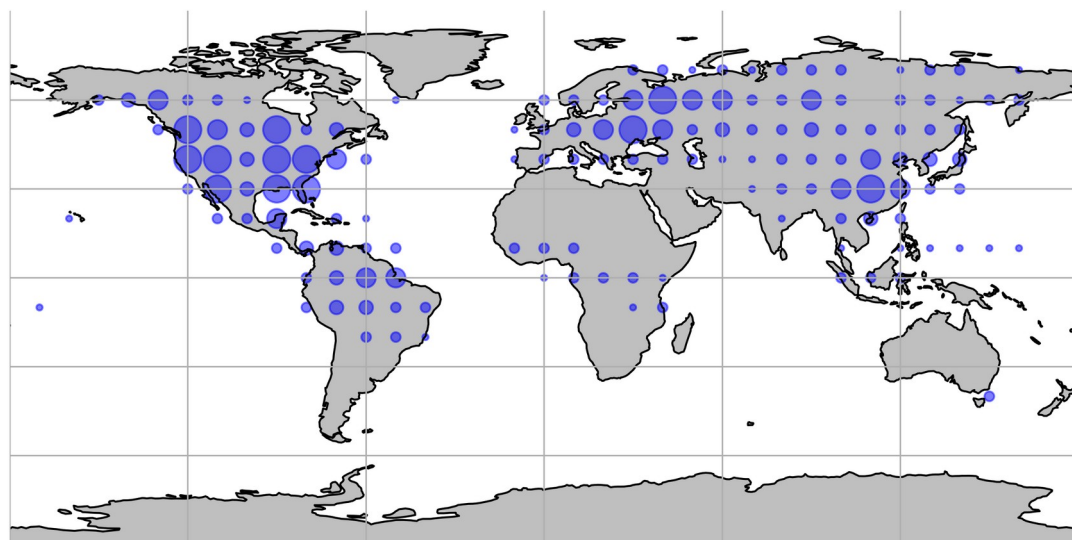
109

110

111

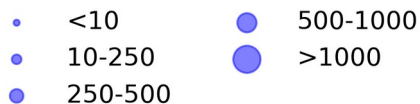
112

113



114

Number of plots



115

116

117

118

119 | **Figure 1** Spatial distribution of the forest inventory plots used for the forest age maps. Each dot represents the total
120 | number of plots within 10x10 degrees.

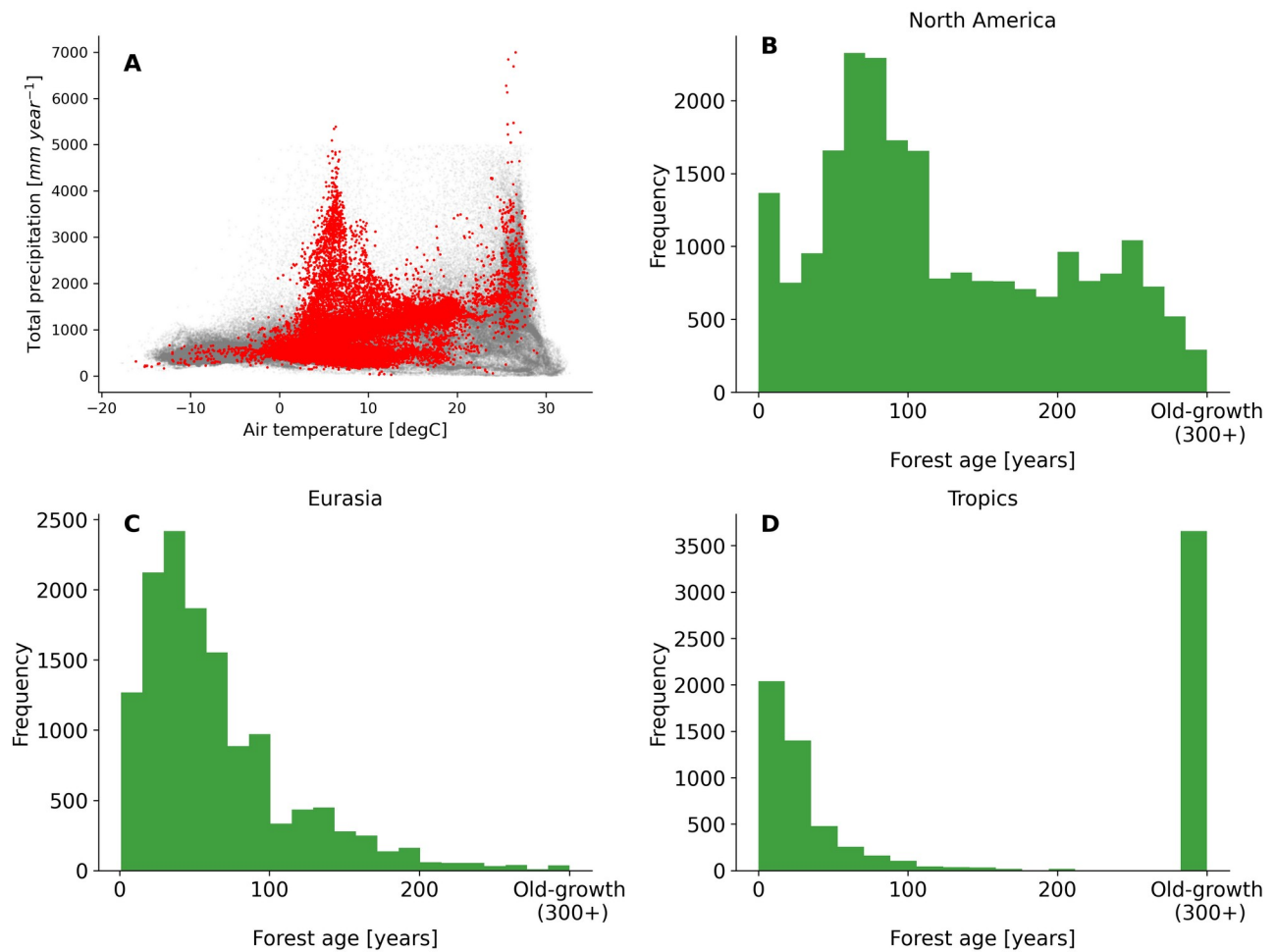
121

122 | A [broadcomprehensive](#) meta-analysis of the compiled dataset (Fig. 2) revealed that the observations covered a large
123 | spectrum in the climate-space (Fig. 2A), although in hot and dry regions, few plots were collected, probably due to the
124 | low presence of forest ecosystems in such regions. We further described the age spectrum covered at the regional scale
125 | and found that a large spectrum of forest age was covered in North America (Fig. 2B) and Eurasia (Fig. 2C), while in
126 | the tropics, biases were observed (i.e., a [largesignificant](#) fraction of tropical old-growth forest and relatively young
127 | forests) (Fig. 2D).

128

129

130



134 **Figure 2** Distribution of the forest inventory plots in a climate space defined by air temperature and total annual
 135 precipitation (A). Histogram distributions of the forest age observations in North America (B), Eurasia (C) and the
 136 tropics (D) are also shown. The grey dots show the global distribution of 0.25° grid-cell forest in climate space defined
 137 by air temperature and precipitation, while the red dots show the distribution of the forest inventory data in the same
 138 climate space.

139

140 For each forest inventory plot, we extracted bioclimatic variables from the WorldClim version2 (Fick and Hijmans,
 141 2017). [In addition, we extracted all the soil-related variables of the Harmonized World Soil Database v 1.2 dataset.](#)
 142 [Finally, we derived a series of proxies for disturbance and management regimes from the Hansen tree cover dataset](#)
 143 [\(Hansen et al., 2010, Science\):](#)

- 144 > [The intensity of tree loss from the Hansen tree cover loss layer \(Hansen et al., 2010, Science\). This metric was](#)
 145 [derived by counting the 30m pixels that experienced a tree cover loss for 2000-2019 within a 1km gridcell.](#)
- 146 > [Last time since tree cover loss from Hansen tree cover loss layer \(Hansen et al., 2010, Science\) – standard](#)
 147 [deviation metric. This metric was calculated as the last time from 2019 since a 30m pixel experienced tree](#)
 148 [cover loss and we further computed the standard deviation of this last time since tree cover loss within a 1km](#)
 149 [gridcell.](#)

150

151 Table S1 summarizes the list of covariates considered in our study. Two datasets were further created. [First, we created](#)
152 [A non-old-growth forests a](#) dataset that contained the plots with a reported stand age estimates ranging from 1 to 299
153 years ([hereafter non-old-growth forests dataset](#)). [Second, we created](#) ~~old and~~ a binary dataset reporting whether an
154 observation had an age estimate less than 300 years ~~-old~~ or whether an observation had an age estimate more than or
155 equal to 300 years ~~-old~~ or not reported but considered as old-growth tropical forests (0= non-old-growth forest and 1=
156 old-growth forest) ([hereafter old-growth dataset](#)).

157 2.2 Feature selection and model training

158 From the set of predictors related to vegetation and climatic conditions (Table S1), we performed a feature ranking with
159 recursive feature elimination (RFE) procedure
160 (https://scikit-learn.org/stable/modules/generated/sklearn.feature_selection.RFE.html) (Guyon et al., 2002) both on the
161 non-old-growth forest and binary datasets. The ~~10~~^{ten} best covariates selected by the RFE algorithm were further used to
162 train either a Random Forest (RF) regressor algorithm (RFRegressor)
163 (<https://scikit-learn.org/stable/modules/generated/sklearn.ensemble.RandomForestRegressor.html>) or an RF classifier
164 algorithm (RFClassifier)
165 (<https://scikit-learn.org/stable/modules/generated/sklearn.ensemble.RandomForestClassifier.html>). As such, two distinct
166 models were implemented. The RFRegressor model was used to estimate forest age in the non-old-growth forests
167 dataset, while the RFClassifier model was used to classify old-growth vs. non-old-growth forests using the binary
168 dataset (0= non-old-growth forest and 1= old-growth forest). The performances of the two models were assessed using
169 leave-one-cluster-out cross-validation to reduce possible spatial auto-correlation between the training and test sets
170 (Ploton et al., 2020). A cluster of plots contained all the plots ~~that were~~ within the same pair of latitude and longitude
171 coordinates rounded to the nearest 10th degree (e.g., latitude= 20 degrees and longitude= 110 degrees) (see Fig. 1). For
172 the RFRegressor model, the root-mean-square error (RMSE), the normalized root-mean-square error (NRMSE) and
173 Nash-Sutcliffe model efficiency coefficient (NSE) were used for assessing the predictive capacity of the model for
174 predicting forest age. For the RFClassifier model, we reported the precision (i.e., the number of correctly-identified
175 members of a class divided by all the times the model predicted that class), recall (i.e., the number of members of a
176 class that the classifier identified correctly divided by the total number of members in that class) metrics, and F1-score
177 (i.e., ~~the combination of precision and recall~~ [for assessing the predictive capacity of the classifier for distinguishing](#)
178 [between old-growth and non-old-growth forests](#)). Additionally, we explored functional relationships between the
179 variables selected by the feature selection procedure and stand age in the RFRegressor model by using the Tree SHapley
180 Additive exPlanations (TreeSHAP) algorithm (Lundberg and Lee, 2017; Lundberg et al., 2018). A negative SHAP value
181 for a given variable X translates a negative contribution to the local changes of forest age; and vice-versa.

182 2.3 Upscaling procedure

183 To upscale the two [trained](#) models (i.e., RFClassifier and RFRegressor models) from plot-level data to the global scale,
184 we collected climate grids from the WorldClim dataset (Fick and Hijmans, 2017) and a series of AGB grids *circa* 2010
185 (i.e., corrected for tree cover with thresholds of 0%, 10%, 20% and 30%) from the Globbiomass project
186 (<http://globbiomass.org/>). The tree cover correction was done by masking ~~-~~ out the 100-meter pixels in the original AGB
187 product (i.e., 100m resolution) having tree cover estimates (Hansen et al., 2013) below one of the [aforementioned](#) tree
188 cover thresholds [mentioned above](#) within a 1km extent. The original filtered AGB maps were [further](#) aggregated from
189 100m to 1km spatial resolution using a bilinear resampling method.

190 | The upscaling procedure was done in two steps. First, each 1km pixel was classified **either** as old-growth or non-old
 191 | growth forests using the trained RFclassifier model. Second, the 1km pixels classified as non-old growth were assigned
 192 | with an age estimate ranging from 0-299 years inferred from the RFregression model, while the pixels classified as old-
 193 | growth forest were assigned a default age value of 300 years. In total, four gridded forest age maps with a 1km spatial
 194 | resolution were obtained using the different **mentioned** AGB maps derived from the different tree cover thresholds
 195 | **as mentioned above** (hereafter MPI-BGC forest age datasets). **From the 1km resolution forest age maps, w**We also
 196 | created maps **from the 1km resolution forest age maps**-that reflected the fraction of several age classes (0-300+ with
 197 | decadal resolution) within each 0.5-degree grid cell resolution.

198 | 3 Results and discussion

199 | 3.1 Model development and evaluation

200 | We used the **10**ten most -important -variables from the set **of variables** presented in Table S1 **identified**identified by the
 201 | RFE algorithm procedure for the RFregression and the RFclassifier models (Table 1). This set of selected variables was
 202 | further used to train the two models **both** in the cross-validation analysis and the global upscaling procedure.

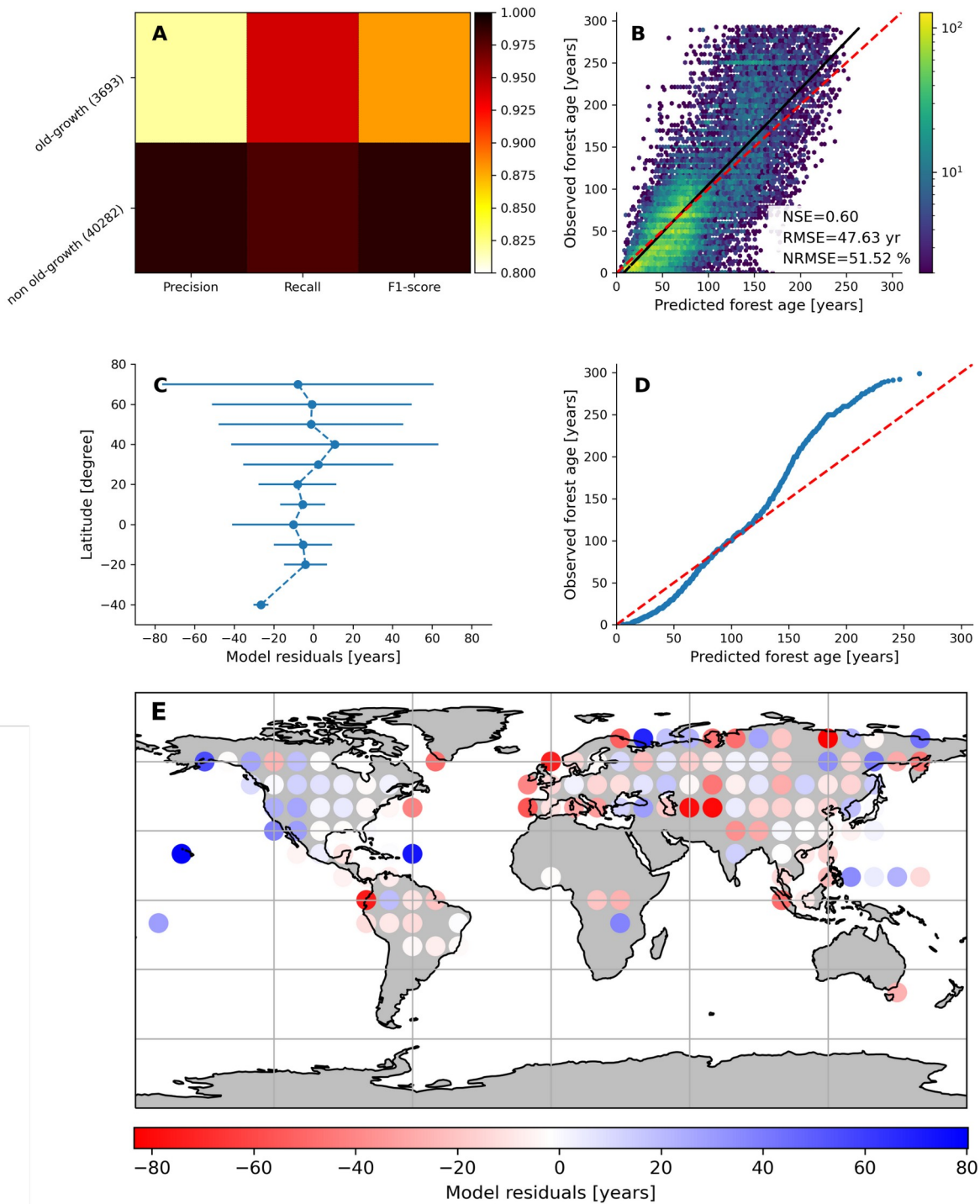
203 | **Table 1** List of the predictors confirmed as important by the feature selection algorithm for RFregression and the
 204 | RFclassifier models. See table S1 for details on the variable names.

| Model setup | Vegetation variables | ClimateHydro-meteorological variables |
|--------------|----------------------|---------------------------------------------------------------------------------------------------------------------------------------------------------------------------------------------------------------|
| RFregression | agb | Isothermality, MaxTemperatureofWarmestMonth, MeanDiurnalRange, MeanTemperatureofWettestQuarter, PrecipitationofWarmestQuarter, PrecipitationofWettestMonth, PrecipitationSeasonality, srاد, vapr |
| RFclassifier | agb | AnnualMeanTemperature, AnnualPrecipitation,Isothermality, MeanTemperatureofColdestQuarter, MeanTemperatureofDriestQuarter, MinTemperatureofColdestMonth, TemperatureAnnualRange, TemperatureSeasonality, vapr |

205

206 | By assessing the cross-validation results, we found that the RFclassifier model **was-able-to**could accurately partition
 207 | old-growth and non-old-growth forests with precision estimates of 0.81 and 0.99 for old-growth **forest** and non-old-
 208 | growth forests, respectively (Fig. 3A). Furthermore, we found recall values of 0.94 and 0.98 for old-growth **forest** and
 209 | non-old-growth forests, respectively, while we found F1-scores of 0.87 and 0.99 for old-growth **forest** and non-old-
 210 | growth forests, respectively (Fig. 3A). The performance of the RFregression model was relatively high (NSE= 0.60,
 211 | RMSE= 47.63 years and NRMSE = 51.52%) (Fig. 3B), while the model residuals across 10-degree latitudinal averages
 212 | were relatively low (Fig. 3C). However, the quantile-quantile plot depicted biases in both very young and old forests
 213 | (Fig. 3D). More precisely, the RFregression model slightly overestimated the age estimates of young forests while **it**
 214 | **underestimated** the age estimates of older forests (i.e., >150 years old) at the plot level. The biases for the very
 215 | young or the older forests were probably due to either the properties of the training dataset in which older forests are
 216 | still largely underrepresented compared to younger stands (Fig. 2A-C) or the statistical method used (i.e., _Random

217 Forests). Such biases could potentially be propagated from plot level to global scale and have implications in
 218 representing the location of younger and older forests globally. [Figure 3E shows the spatial patterns of the model](#)
 219 [residuals. For instance, we observed that the RRegression model underestimated the age estimates in most North](#)
 220 [American forests while overestimated the age estimates in most European forests.](#)



222

223

224

225

226 |
227 |
228 |
229 |
230 |
231 |
232 |
233 |
234 |
235 |
236 |
237 |
238 |
239 |
240 |
241 |
242 |
243 |
244 |
245 |
246 |
247 |
248 |
249 |
250 |
251 |
252 |
253 |
254 |
255 |
256 |
257 |
258 |
259 |
260 |
261 |
262 |
263 |
264 |
265 |

Figure 3 Cross-validated results of the old-forests vs. non-old-forests classification (A) and comparison of predicted vs. observed forest age estimates from the regression model (B). In C, the average model residuals \mp standard deviation within 10-degree latitudinal beans ~~are~~ shown. The quantile-quantile plot (D) is also shown.

We further investigated the variable importance of the selected variables and the functional relationships learned by the RF regression model between forest age and these selected variables. For this, we computed the SHAP values for each predictor to show how each predictor contributes, either positively or negatively, to the forest age estimates. First of all, we observed that *vapr* was the most important variable, followed by *agb* and *MeanTemperatureWettestQuarter* (Fig. 4). Biomass estimates contain information about the current state of the forest, integrating the cumulative effect of land-use change, management and disturbance history. Having biomass (i.e., *agb*) as an important variable in predicting forest age confirmed strong controls of management and disturbance regimes on the forest age distribution (ref). While it was expected to have biomass (i.e., *agb*) as an important variable in predicting forest age, it was interesting to find that a proxy for atmospheric water demand (i.e., *vapr*) had a strong substantial control on forest age. Such The high importance of atmospheric water demand in explaining stand age variability could indicate how biomass is associated with stand age across different climate regimes. More precisely, such observations could imply that high atmospheric water demand limits growth rates and maximum biomass, thereby indirectly controlling how biomass relates to age. In addition, high atmospheric water demand might influence fire frequency (Mueller et al., 2020) and indirectly control forest age distribution through the effect of fire on biomass. *vapr* could suggest, for instance, an association between high atmospheric demand for water (i.e., dry conditions) and disturbance intervals (e.g., fire frequency) (Mueller et al., 2020), therefore impacting the age distribution at the plot level.

266

267

268

269

270

271

272

273

274

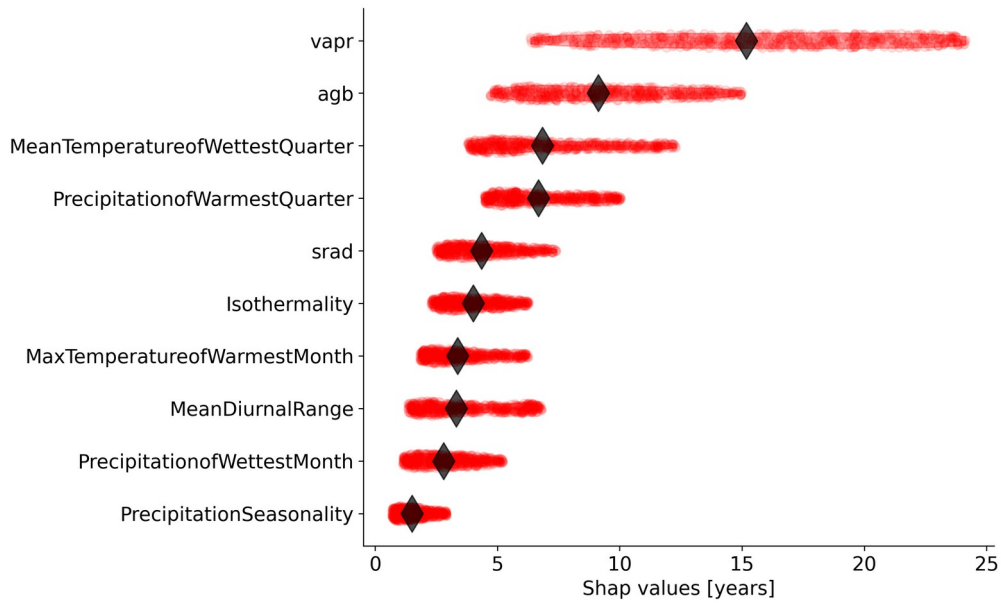
275

276

277

278

279

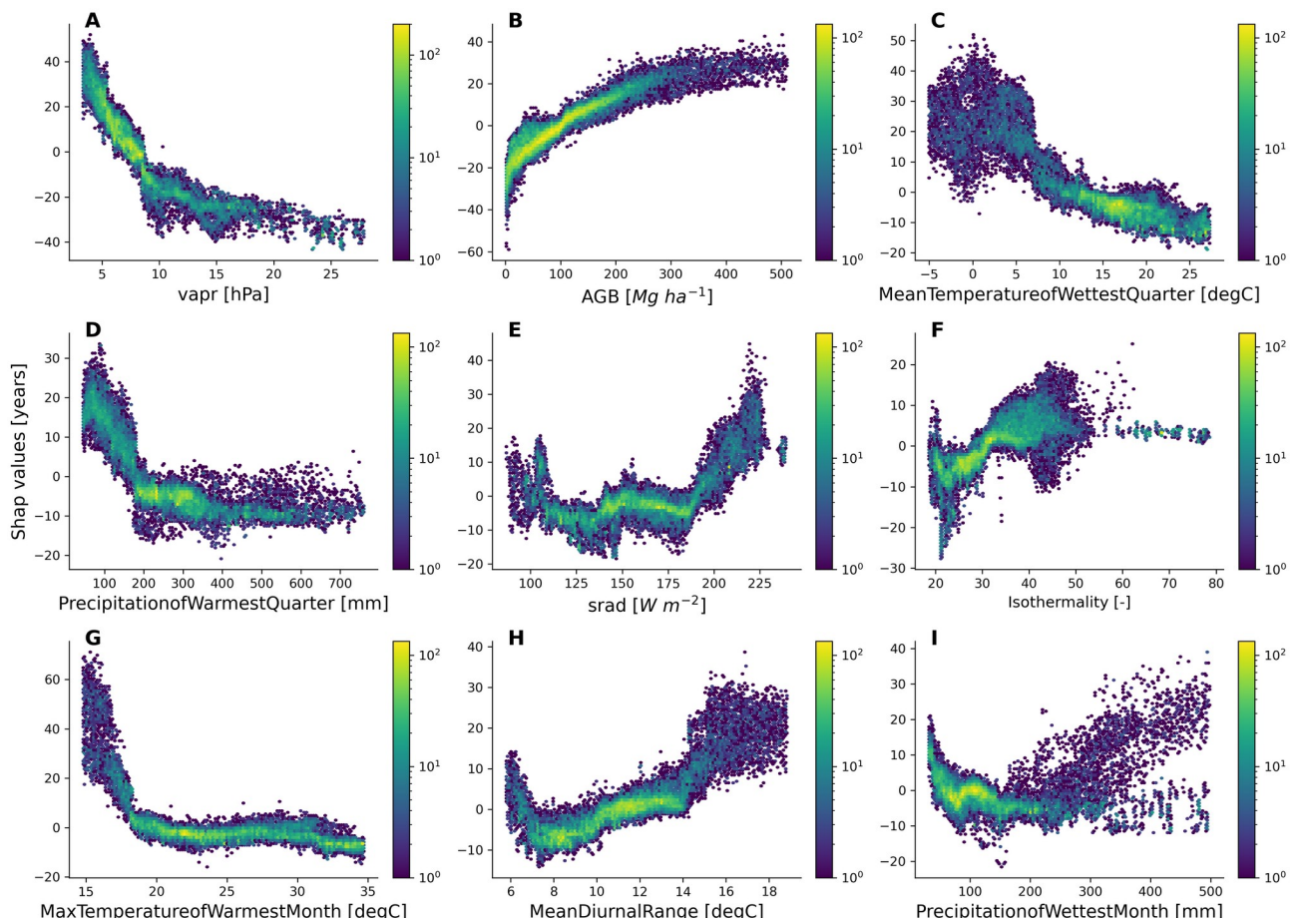


281 **Figure 4** Relative importance of the independent variables selected by the feature selection algorithm in predicting
 282 forest age estimates in the RF regression model. Each dot represents the absolute SHAP value of one observation. The
 283 diamond represents the median value for each variable.

284

285 The emergent relationships revealed that an increase in AGB was associated with an increase in the forest age estimates
 286 (Fig. 5A). This was expected as older trees have a higher amount of carbon stored in the aboveground components
 287 compared to younger forests. Such a relationship was expected as older trees have more carbon stored in the
 288 aboveground components than younger forests. The ~~modelled~~ modeled forest age estimates appeared to be also
 289 relatively sensitive to the climatic conditions. For instance, we observed that climatic conditions with low water
 290 atmospheric demand (i.e., low vapr) (Fig. 5C) promoted older forests as well as or conditions with high solar radiation
 291 (Fig. 5E), such as in the wet tropics increased forest age. Finally Similarly, we observed that changes in forest age
 292 variability were also associated with air temperature conditions (Fig. 5E-G) and precipitation regimes (Fig. 5H and
 293 Fig. 5I).

294



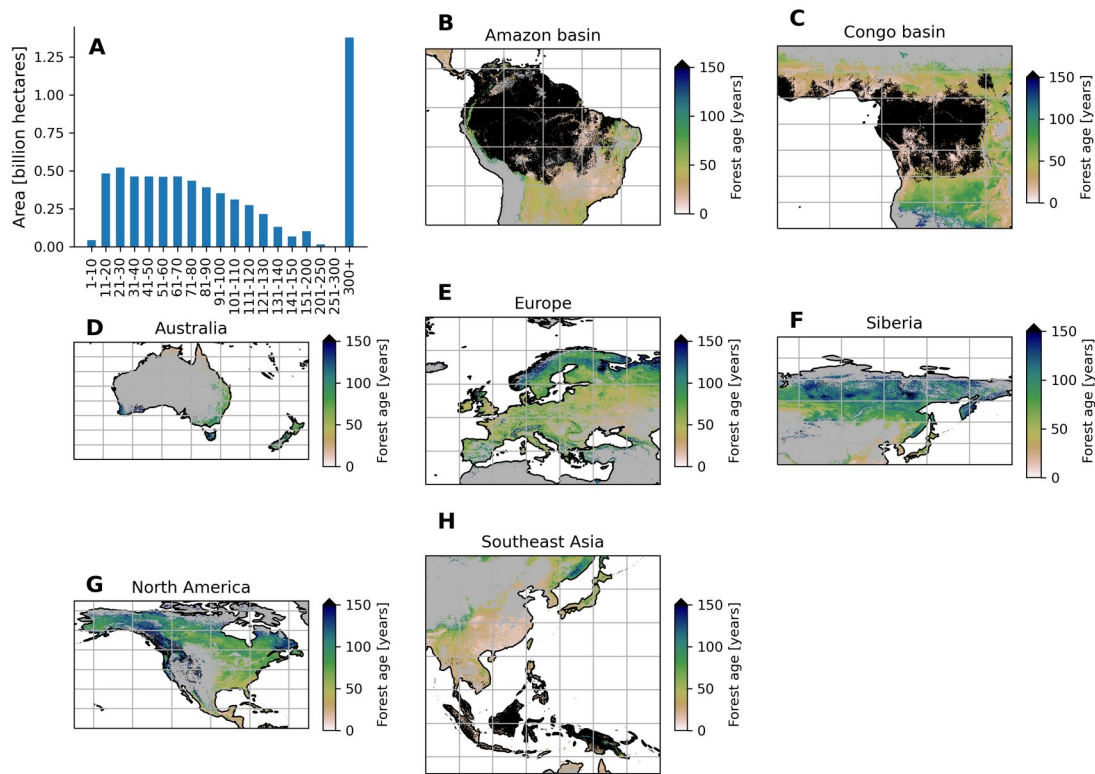
296 **Figure 5** Emergent relationships between the retrieved SHAP values and the independent variables selected by the
 297 feature selection algorithm.

298

299 3.2 Global forest age patterns and regional overview

300 The MPI-BGC forest age product shows a large range of forest age across the globe (Fig. 6). We observed that the most
 301 represented age class was the old-growth forests with around 1,1 billion hectares, while a limited fraction of very young
 302 forest was observed (i.e., < 10 years old) (Fig. 6A). Not surprisingly, most of the old-growth/undisturbed forests (+300
 303 years old) can be found in the Amazon basin (Fig. 6B), the Congo basin (Fig. 6C) and part of the Indonesian peninsula
 304 (Fig. 6H), where the minimal human disturbance occurred. A large area occupied by very young forests was found in
 305 the Southeast part of China (Fig. 6H), probably due to the implementation of afforestation/reforestation policies as well
 306 as and natural disturbances (Zhang et al., 2017). Similarly, young and intermediate forests were found in the African
 307 tropical dry forests (i.e., Sahel and Miombo regions) (Fig. 6C), where the frequency of the fire regimes is very high,
 308 resulting in a relatively young age-class structure (Werf et al., 2017). Large scale fires in the North American boreal
 309 region also resulted in widespread patches of younger forests as well as and a mosaic of stands of different ages since
 310 they last burned (Fig. 6G). On the other hand Furthermore, the unmanaged part of the North American boreal region
 311 near the ecotone, where fires are more infrequent, revealed older stands (Fig. 6G). Forests in British Columbia were
 312 generally old, although patches of younger forests probably in the early stages of recovery from disturbance were also
 313 observed. Forests in British Columbia were generally old, although patches of younger forests were probably in the early
 314 stages of disturbance recovery. European forests were in young/intermediate stages of forest succession (Fig. 6E). The
 315 increase of harvested forest area (Ceccherini et al., 2020) and considerable afforestation practices (Naudts, et al., 2016)

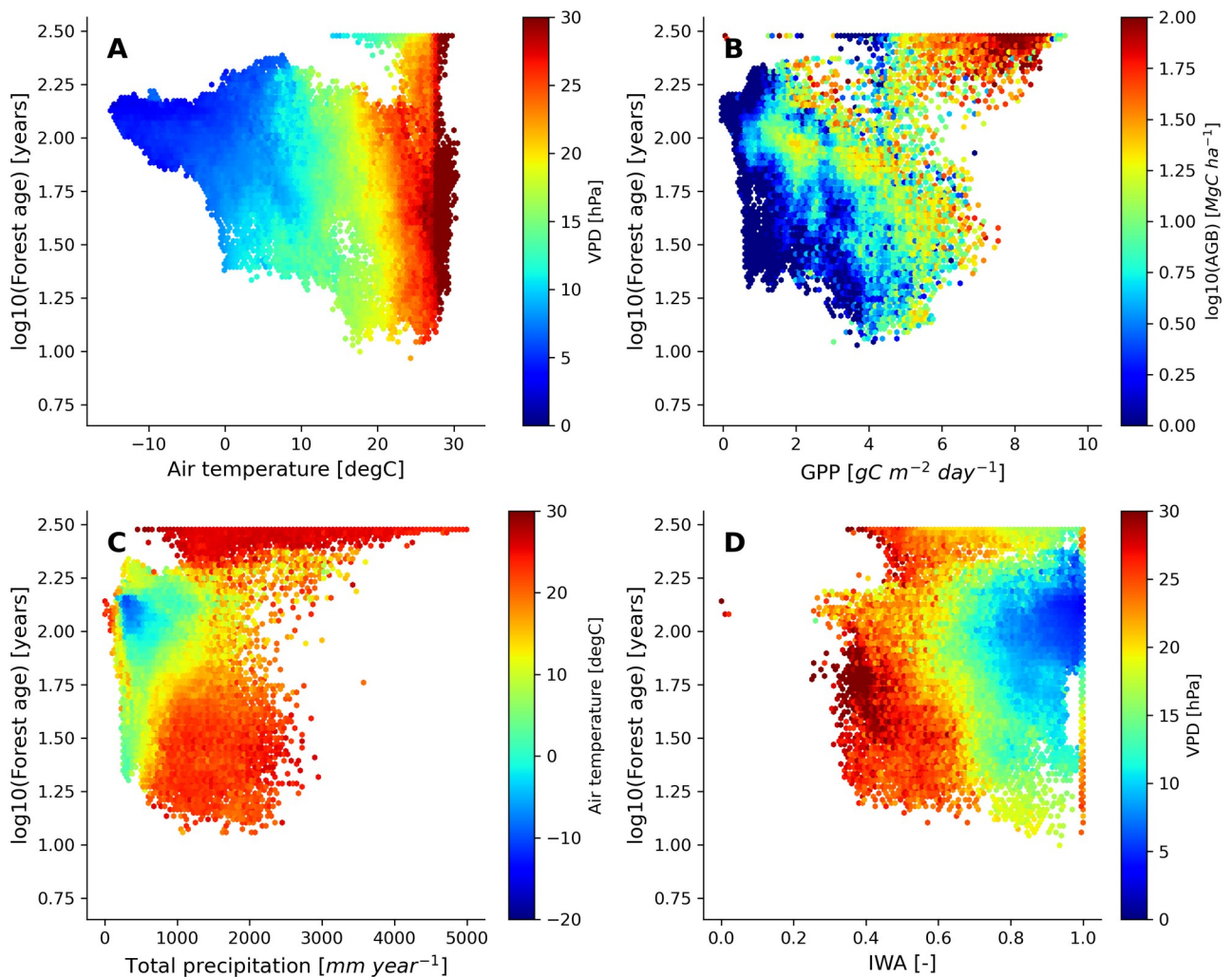
316 were probably explaining a relatively young to intermediate forest demography as well as a mosaic of different age
 317 classes in the European region. The increase of harvested forest area and considerable afforestation practices (Naudts, et
 318 al., 2016) probably explained a relatively young to intermediate forest demography and a mosaic of different age classes
 319 in the European region. The region of Siberia revealed a gradient of younger to older forests going from the South to the
 320 North part of the Siberian region (Fig. 6F). Such an observation could suggest different fire regimes between Southern
 321 and Northern Siberia (Shorohova et al., 2011) and confirm harvesting practices identified in Southern Siberia (Curtis et
 322 al., 2018). Finally, Australian forests were relatively young in the North part of the country while a mosaic of age class
 323 dominated the Southern part of Australia (Fig. 6D). The age patterns observed in the Northern part of Australia
 324 somehow correspond to the fact that forests are defined as regrowth in this region (Pugh et al., 2019). Yet However, it is
 325 important essential to note that the few forest inventory plots in regions such as Australia (Fig. 1) could limit our
 326 certainty on the forest age estimates attributed by the statistical approaches due to extrapolation issues. Finally, we
 327 assumed forest homogeneity within a 1 km grid-cell, which would reduce the extremes of low and high biomass
 328 estimates in the gridded global products that the models have learned in the plot-level training data. This limitation
 329 might, for instance, explain the relative dearth of very young stands (1-10 years old) in the MPI-BGC global age
 330 product (Figs.6A).



350 **Figure 6** Total area of each age class globally (A) and close-up examples in the Amazon Basin (B), Congo Basin (C),
 351 Australia (D), Europe (E), Siberia (F), North America (G) and Southeast Asia (H). For better visualization, the forest
 352 age estimates in the close-up examples (B-H) range from 0 to 150 years old. The forest age estimates in the close-up
 353 examples (B-H) range from 0 to 150 years old for better visualisation. The forest age map using a 10% tree cover
 354 threshold is shown.

356 3.3 Global forest age relationships with atmosphere, hydrosphere and vegetation conditions

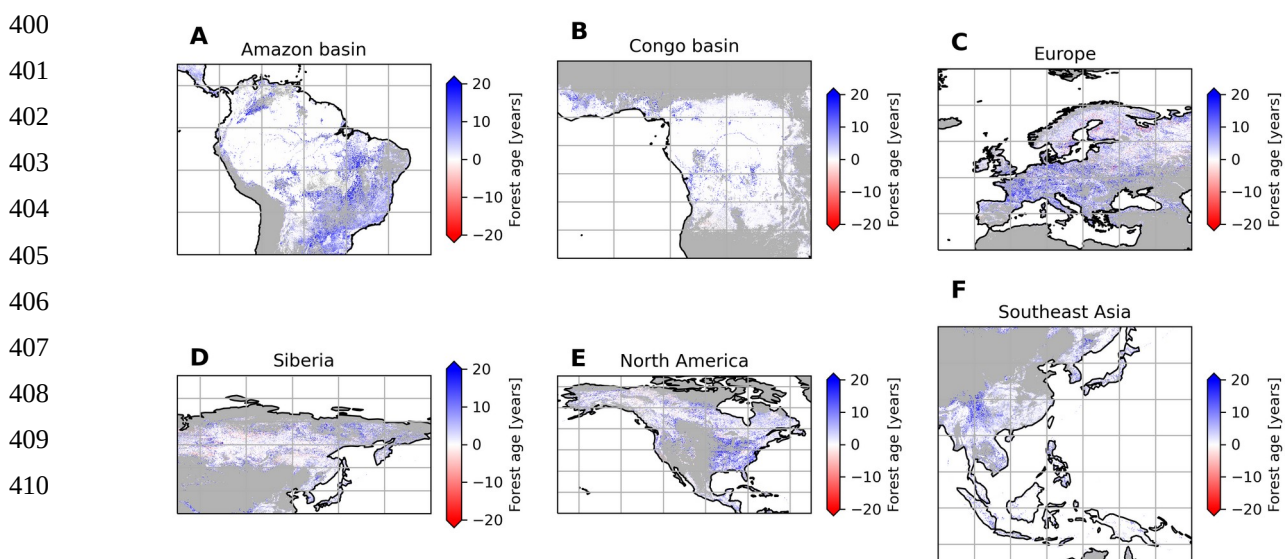
357 We further investigated the distribution of the forest demography in the climate and vegetation spaces (Fig. 7).
358 Generally, we observed that with warmer (i.e., air temperature) and drier (i.e., VPD) conditions, forests appeared to be
359 younger with the expectation of old-growth tropical forests located in relatively warm climatic conditions (Fig. 7A).
360 Not surprisingly, we found that most of the old-growth tropical forests were located in regions with high productivity
361 (i.e., high GPP and high biomass) (Fig. 7B), which coincides with our previous results investigating the structure of the
362 statistical model showing that an increase in forest biomass was coupled with an increase in forest age (Fig. 5A). On the
363 other hand, we observed that younger-intermediate forests were more productive than older forests outside the tropical
364 old-growth forest envelope. ~~More precisely, for similar carbon stocks, we found that forest being less productive will~~
365 ~~tend to belong to an older age class.~~ More precisely, we found that forests being less productive will belong to an older
366 age class for similar carbon stocks. Mature forests were found in cool temperatures and moderately low precipitation
367 conditions (Fig. 7C), where rates of fast growth but slow decomposition generally drive forest dynamics, ~~therefore~~
368 ~~where mature forests can potentially be found.~~ On the other hand, younger stands, on the other hand,
369 in relatively warm conditions but in a wide range of precipitation regimes (Fig. 7C). Finally, while a large significant
370 fraction of young forests were located in regions with low water availability and high water atmospheric demands, we
371 also observed that above a certain threshold of water availability (i.e., > 0.4-0.5), the amount of water available for trees
372 (i.e., IWA) was not directly associated with changes in forest age unlike VPD (Fig. 7D).
373



375 | **Figure 7** Forest age distribution in the climate, hydrological and productivity spaces defined by air temperature, vapour
 376 pressure deficit, total precipitation, soil water availability, GPP and above-ground biomass. The forest age map used
 377 here corresponds to a tree cover threshold of 10% aggregated to 0.25 degree using a weighted average of all non-
 378 NODATA contributing pixels. GPP is gross primary productivity derived from the FLUXCOM RS+meteo product
 379 (Tramontana et al. 2016; Jung et al. 2011; Jung et al. 2020), and IWA is an index for soil water availability (Tramontana
 380 et al. 2016). The climatic variables were retrieved from the ERA5-reanalysis data
 381 (<https://apps.ecmwf.int/datasets/licences/copernicus/>). For all the climatic variables, we computed an annual mean for
 382 the year 2010.

383 3.4 Sensitivity analysis, uncertainties and comparison with previous products

384 We performed a sensitivity analysis using a series of AGB gridded products filtered with different tree cover thresholds
 385 to produce different global age products (see method section) (Fig. 8). This analysis showed that in South America,
 386 mainly the dry regions were sensitive to the tree cover threshold being applied, with forest age estimates being lower
 387 when no tree cover threshold was applied compared to a 30% tree cover correction (Fig. 8A). Similarly, we observed
 388 that the dry parts of the Congo basin depicted a sensitivity to the applied tree cover thresholds (Fig. 8B). In Europe, we
 389 observed widespread differences between the forest age estimated without a tree cover correction and with a tree cover
 390 correction (Fig. 8C). Generally, forest age estimates were higher when the 30% tree cover correction was applied. In
 391 Siberia (Fig. 8D), North America (Fig. 8E) and Southeast Asia (Fig. 8F), there were also large patches of forest where
 392 correcting the biomass maps with a tree cover threshold led to substantial differences in the age estimates. Overall, such
 393 observations were expected ~~as mosaic vegetation, due to because of~~ management practices or disturbance regimes,
 394 resulting in mosaic vegetation within a 1km grid cell. Such mosaic vegetation in regions such as the dry tropics
 395 (forest/grassland/shrubland), Europe (forests/croplands) and Northeast of the United States (forests/croplands) could
 396 explain the sensitivity of the forest age estimates to tree cover thresholds in these regions. in the dry tropics
 397 (forest/grassland/shrubland), in Europe (forests/croplands) and Northeast of the United States (forests/croplands) are
 398 largely represented within a 1km grid cell, which could explain the sensitivity of the forest age estimates to tree cover
 399 thresholds in these regions.



411 **Figure 8** Sensitivity of the presented age product using 30% tree cover correction thresholds or no tree cover correction.
 412 The differences between the age estimates derived from a forest biomass product using a 30% tree cover correction and

413 the age estimates derived from a forest biomass product not using a tree cover correction are shown. Blue colour means
414 that the age estimates are higher with the 30% tree cover correction than without correction, while the red colour means
415 that the age estimates are lower with the 30% tree cover correction than without correction.

416

417 Besides, we explored uncertainties associated with the two statistical models used for the upscaling procedure (Fig. S1,
418 Fig. S2 and Fig. S3). ~~First, we observed that the RFclassifier model had overall very high probabilities to classify a non-~~
419 ~~old-growth forest pixel when being classified as a non-old-growth forest (Fig. S1), and vice-versa (Fig. S2), suggesting~~
420 ~~relatively high confidence in the partitioning between old-growth and non-old-growth forests in the MPI-BGC forest~~
421 ~~age product.~~First, we observed that the RFclassifier model had very high probabilities of classifying either a non-old-
422 growth or an old-growth forest at pixel level as the fraction of the random forest ensemble to classify the two forest
423 classes was generally close to one. (Fig. S1 and Fig. S2), suggesting relatively high confidence in the partitioning
424 between old-growth and non-old-growth forests in the MPI-BGC forest age product. The regions at the edge of the
425 Amazon and the Congo basins appeared to have the lowest confidence in classifying old-growth vs. non-old-growth
426 forests (Fig. S1A, Fig. S1B and Fig. S2) with a probability close to 0.5. On the other hand, we observed relatively high
427 probabilities for classifying non-old-growth forests in Europe (Fig. S1C), Siberia (Fig. S1D), North America (Fig. S1E)
428 and Southeast Asia (Fig. S1F). We also provided uncertainties in predicting forest age estimates by retrieving the 25%,
429 50%, and 75% quantile predictions from the RFregressor model for computing the inter-quantile range (IQR, quantile
430 75% - quantile 25%) divided by the median (i.e., quantile 50%) of the forest age estimates (IQR/median) (Fig. S3).
431 While in Europe (Fig. S3C), China (Fig. S3F) and the Eastern United States (Fig. S3E), the IQR/median estimates were
432 relatively low, we observed high IQR/median estimates in Northern North American regions (Fig. S3E) as well as in
433 large patches of Siberia (Fig. S3D) and the dry tropics (Fig. S3A and Fig. S3F).

434 We further compared the spatial patterns of the MPI-BGC forest age dataset with a series of independent regional and
435 global forest age products (Chazdon et al., 2016; Pan et al., 2011; Poulter et al., 2019; Zhang et al., 2017) (Fig. 9, ~~and~~
436 ~~Fig. 10, and Fig. S7~~). In the Amazon basin, we found that the MPI-BGC forest age product depicted widespread higher
437 forest age estimates (i.e., blue colour) than the Chazdon et al. (2016) dataset (Fig. 9A), resulting in a ~~s~~ubstantially
438 bigger more extensive area of tropical old-growth forest in the MPI-BGC forest age product (Fig. 9B). On the other
439 hand, we observed lower forest age estimates in the regions of Rio Grande Do Norte and Paraiba in the MPI-BGC forest
440 age product (i.e., red colour). Such disagreement between the two products could be related not only to the different
441 methods used to infer forest age (i.e., statistical method vs. age-AGB chronosequence approach for the MPI-BGC forest
442 age and the Chazdon products, respectively) but also to the uncertainties of the RFclassifier for classifying old-growth
443 vs. non-old-growth forests in this region (Fig. S1 and Fig. S2). Similarly, the presented product and the Pan et al. (2011)
444 dataset revealed widespread discrepancies in the North American region, particularly in the Western part of the United
445 States and the North American boreal forests (Fig. 8E). More precisely, the Pan et al. (2011) dataset had a higher
446 fraction of young forest patches than the MPI-BGC forest age product (Fig. 9F). Methodological differences between
447 the Pan et al. (2011) and the MPI-BGC forest age datasets could explain such differences. While the Pan et al. (2011)
448 dataset integrate forest inventories, disturbance datasets, and land-use/land cover change data forest inventory, fire
449 polygon data and remote sensing and a multi-stage approach were used to retrieve forest age estimates in the Pan et al.
450 (2011) dataset, the MPI-BGC forest age product relied on forest inventory ~~and~~, climate data ~~as well as~~and statistical
451 methods. Additionally, forest inventory plots used to derive the MPI-BGC forest age product were relatively sparse in
452 Canada (Fig. 1), which might limit the statistical methods used for the MPI-BGC forest age product to predict realistic
453 forest age estimates (i.e., extrapolation issues). The fact that the Pan et al. (2011) dataset relies mainly on disturbances

454 regimes inferred from optical remote sensing data (not biomass estimates) might explain the relatively higher fraction of
 455 young forests in the Pan et al. (2011) dataset compared to the MPI-BGC dataset. Finally, the forest age estimates of the
 456 MPI-BGC forest age product in China were rather consistent with the Zhang et al. (2017) dataset (Fig. 9C). The area
 457 distribution across age classes of the two products appeared to have a relatively good agreement in China (Fig. 9D).

458

459

460

461

462

463

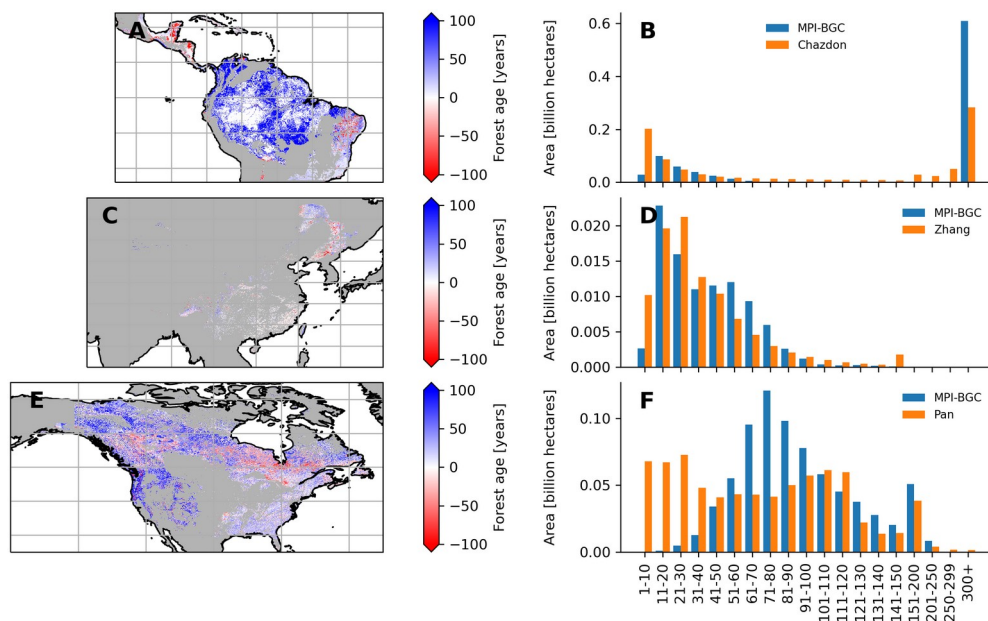
464

465

466

467

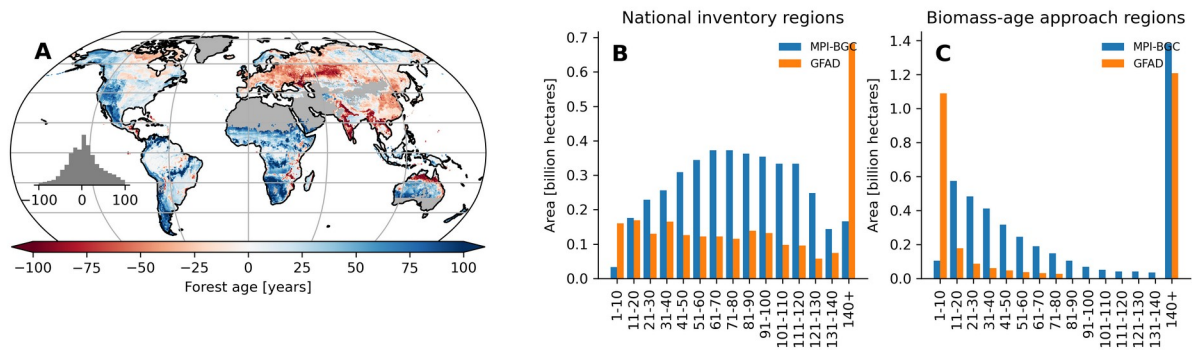
468



469 **Figure 9** Comparison between the forest age dataset from this study and independent forest age dataset: Amazon basin
 470 (A and B), China (C and D) and North America (E and F). For a fair comparison with the independent age datasets, the
 471 MPI-BGC forest age map used here is the one without tree cover correction applied to the AGB dataset. Differences
 472 were computed using weighted age estimates from the fraction of the decadal age classes within each 0.5-degree grid
 473 cell resolution.

474 We also found **largesignificant** and widespread discrepancies between the MPI-BGC forest age dataset and the global
 475 forest age dataset (GFAD) (Poulter et al., 2019) (Fig. 10). Overall, the GFAD product had **both** higher fractions of very
 476 young **forests** and old forests (Fig. 10B). Because the GFAD used a different AGB product for the pan-tropical region
 477 and mainly relied on **coarse national forest inventory data summaries of statistics from national forest inventories**
 478 for the Northern hemisphere, widespread differences were expected between the GFAD and the MPI-BGC forest age maps.
 479 For instance, the MPI-BGC forest age dataset depicted older forests in the Western part of the United States (i.e., blue
 480 colour), while it showed younger forests across Europe than the GFAD product (Fig. 10A). Differences were also
 481 apparent in the dry tropics, where **the GFAD product showed younger forests than** the MPI-BGC forest age dataset
 482 **showed younger forests than the GFAD product**, particularly in the Miombo regions. Such observations could be
 483 explained **either by the use of a biomass-age approach in this region or** by the integration of MODIS fire information in
 484 the GFAD forest age dataset. **As such, w**We adjusted the MPI-BGC forest age dataset with the forest age product
 485 inferred from the MCD45A1 MODerate-resolution Imaging Spectroradiometer (MODIS) fire product at 1 km
 486 resolution (Giglio et al., 2018, Poulter et al., 2019), which was used in the GFAD product. In this MODIS-age product,
 487 forest age was determined as the last time since a fire event occurred **w**ithin a grid cell for **the period** 2000-2015,
 488 thereby assuming that the entire pixel was burned down. For instance, forest age within a 1 km grid cell was **5**five
 489 old if the last time a fire occurred within this grid cell was in 2010. **When adjusting the MPI-BGC forest age dataset**
 490 **with the MODIS-age product, the latter took precedence over the former dataset****The latter took precedence over the**

491 former dataset when adjusting the MPI-BGC forest age dataset with the MODIS-age product. As expected, we
 492 observed a higher fraction of younger forest in the adjusted MPI-BGC forest age dataset (Fig. S4B), particularly in
 493 regions relying in the biomass-age approach in the GFAD product (Fig. S4A and C). Although However,
 494 largesignificant discrepancies between the two products remained when comparing the weighted average forest age
 495 estimates at the pixel level, particularly in European forests (Fig. S4A). We acknowledge that a comparison between the
 496 GFAD and the MPI-BGC forest age maps has to be taken with caution when evaluating the MPI-BGC product as
 497 substantial methodological differences exist between the two products.
 498



500
501
502
503
504
505
506
507
508

509 **Figure 10** Difference between the forest age estimates derived from the MPI-BGC forest age product and the GFAD
 510 product Difference map between the forest age estimates derived from the MPI-BGC and GFAD products (A). Areas per
 511 age class were also compared between the two products for regions relying on national inventories (B) and relying on
 512 biomass-age approach (C) in the GFAD product. Differences were computed using weighted age estimates from the
 513 fraction of the decadal age classes within each 0.5-degree grid cell resolution.

514 **4 Data availability**

515 The dataset of the different forest age products presented in this study can be downloaded from the Data Portal of the
 516 Max Planck Institute for Biogeochemistry at <https://doi.org/10.17871/ForestAgeBGI.2021> (Besnard et al., 2021). For
 517 anonymous access during review, the data are available at <https://nextcloud.bgc-jena.mpg.de/s/Xwt8AdkHkgL3TTc>.

518 **5 Conclusion**

519 We presented a new forest age dataset derived from forest inventory, biomass, climate and remote sensing data.
520 Generally, the statistical model used to create the gridded age datasets had a relatively good capacity to predict forest
521 age estimates at plot level (precision of 0.81 and 0.99 for classifying old-growth and non-old-growth, respectively and
522 NSE of 0.6 for predicting non-old-growth forests); ~~At the same time, while~~ biases were observed, particularly when
523 predicting older forests. The functional relationships between biomass and forest age learned by the statistical models
524 appeared to agree with forest age theory and the role of environmental/climate in modulating the relationship. The
525 proposed gridded datasets allowed us to assess the global patterns of forest age and provided insights into regional
526 forest demography. ~~For instance, relatively young-intermediate forests were observed in Europe and China where~~
527 ~~management practices and afforestation/reforestation activities are predominant~~For instance, relatively young-
528 intermediate forests were observed in Europe and China, where predominant management practices and
529 afforestation/reforestation activities. We could also demonstrate that old forests are ~~largely~~primarily represented in very
530 wet and warm regions ~~as well as in~~and very cold regions. However, ~~the comparison of~~comparing the MPI-BGC forest
531 age product with independent forest age datasets revealed large discrepancies between them, suggesting high
532 uncertainties in mapping forest demography globally. ~~Overall, this forest age product provides a new source of~~
533 ~~information related to disturbance history and forest regrowth, which is key to achieve a better understanding of the~~
534 ~~location of the forest carbon sinks and sources.~~Overall, this forest age product provides a new source of information
535 related to disturbance history and forest regrowth, which is crucial to better understanding the location of the forest
536 carbon sinks and sources.

537

538 **Author contributions**

539 SB and NC designed the study. SB conducted analysis and wrote the paper under the direction of NC. SB, NC, SK, JG,
540 and UW collected and harmonized the forest inventories datasets. BP, BH, JK, and AN provided data for the analysis.
541 All authors contributed to the discussions and interpretation of the results and the writing of the paper.

542

543 **Competing interests**

544 The authors declare that they have no conflict of interest.

545

546 **Acknowledgments**

547 We would like to thank all the initiatives aiming to collect forest inventory plots. We thank the members of the
548 Biogeochemical Integration Department at the Max Planck Institute for Biogeochemistry for providing feedback on the
549 presented results. We acknowledge support by the European Union through the BIOMASCAT
550 (<https://eo4society.esa.int/projects/biomascats/>) and VERIFY (776810) (<https://cordis.europa.eu/project/id/776810>)
551 projects.

552 **References**

553 Álvarez-Dávila, E., L. Cayuela, S. González-Caro, A. M. Aldana, P. R. Stevenson, O. Phillips, Á. Cogollo, M. C.
554 Peñuela, P. v. Hildebrand, E. Jiménez, O. Melo, A. C. Londoño-Vega, I. Mendoza, O. Velásquez, F. Fernández, M.
555 Serna, C. Velázquez-Rua, D. Benítez, and J. M. Rey-Benayas (2017). "Forest biomass density across large climate

556 gradients in northern South America is related to water availability but not with temperature”. PLOS ONE 12.3,
557 e0171072.

558 Amiro, B. D., A. G. Barr, J. G. Barr, T. A. Black, R. Bracho, M. Brown, J. Chen, K. L. Clark, K. J. Davis, A. R. Desai,
559 S. Dore, V. Engel, J. D. Fuentes, A. H. Goldstein, M. L. Goulden, T. E. Kolb, M. B. Lavigne, B. E. Law, H. A. Margolis,
560 T. Martin, J. H. McCaughey, L. Misson, M. Montes-Helu, A. Noormets, J. T. Randerson, G. Starr, and J. Xiao (2010).
561 “Ecosystem carbon dioxide fluxes after disturbance in forests of North America”. *Journal of Geophysical Research:*
562 *Biogeosciences* 115.G4.

563 Anderson-Teixeira, K. J., M. M. H. Wang, J. C. McGarvey, V. Herrmann, A. J. Tepley, B. Bond- Lamberty, and D. S.
564 LeBauer (2018). “ForC: a global database of forest carbon stocks and fluxes”. *Ecology* 99.6, 1507.

565 Anderson-Teixeira, K. J., M. M. H. Wang, J. C. McGarvey, and D. S. LeBauer (2016). “Carbon dynamics of mature and
566 regrowth tropical forests derived from a pantropical database (TropForC-db)”. *Global Change Biology* 22.5, 1690–
567 1709.

568 Baker, T. R., D. M. V. Díaz, V. C. Moscoso, G. Navarro, A. Monteagudo, R. Pinto, K. Cangani, N. M. Fyllas, G. L.
569 Gonzalez, W. F. Laurance, S. L. Lewis, J. Lloyd, H. t. Steege, J. W. Terborgh, and O. L. Phillips (2016). “Consistent,
570 small effects of treefall disturbances on the composition and diversity of four Amazonian forests”. *Journal of Ecology*
571 104.2, 497–506.

572 Bar-On, YM, Phillips, R., & Milo, R. (2018). The biomass distribution on Earth. *Proceedings of the National Academy*
573 *of Sciences*, 115 (25), 6506-6511.

574 Besnard, S., Koirala, S., Santoro, M., Weber, U., Nelson, J., Gütter, J, Herault, B., Kassi, J., N'Guessan, A., Neigh, C.,
575 Poulter, B., Zhang, T., and Carvahais, N. (2021). The MPI-BGC global forest age datasets, MPI-BGC,
576 <https://doi.org/10.17871/ForestAgeBGI.2021>.

577 Besnard, S., N. Carvahais, M. A. Arain, A. Black, S. d. Bruin, N. Buchmann, A. Cescatti, J. Chen, J. G. P. W. Clevers,
578 A. R. Desai, C. M. Gough, K. Havrankova, M. Herold, L. Hörtnagl, M. Jung, A. Knohl, B. Kruijt, L. Krupkova, B. E.
579 Law, A. Lindroth, A. Noormets, O. Roupsard, R. Steinbrecher, A. Varlagin, C. Vincke, and M. Reichstein (2018).
580 “Quantifying the effect of forest age in annual net forest carbon balance”. *Environmental Research Letters* 13.12,
581 124018.

582 Birdsey, R., K. Pregitzer, and A. Lucier (2006). “Forest carbon management in the United States: 1600-2100”. *Journal*
583 *of Environmental Quality* 35.4, 1461–1469.

584 Bowman, D. M. J. S., J. K. Balch, P. Artaxo, W. J. Bond, J. M. Carlson, M. A. Cochrane, C. M. D’Antonio, R. S.
585 DeFries, J. C. Doyle, S. P. Harrison, F. H. Johnston, J. E. Keeley, M. A. Krawchuk, C. A. Kull, J. B. Marston, M. A.
586 Moritz, I. C. Prentice, C. I. Roos, A. C. Scott, T. W. Swetnam, G. R. v. d. Werf, and S. J. Pyne (2009). “Fire in the Earth
587 System”. *Science* 324.5926, 481–484.

588 Buitenwerf, R., B. Sandel, S. Normand, A. Mimet, and J.-C. Svenning (2018). “Land surface greening suggests
589 vigorous woody regrowth throughout European semi-natural vegetation”. *Global Change Biology* 24.12, 5789–5801.

590 Burrill, Elizabeth A.; Wilson, Andrea M.; Turner, Jeffery A.; Pugh, Scott A.; Menlove, James; Christiansen, Glenn;
591 Conkling, Barbara L.; David, Winnie. 2018. *The Forest Inventory and Analysis Database: database description and user*
592 *guide version 8.0 for Phase 2*. U.S. Department of Agriculture, Forest Service. 946 p.

593 Ceccherini, G., Duveiller, G., Grassi, G., Lemoine, G., Avitabile, V., Pilli, R., & Cescatti, A. (2020). Abrupt increase in
594 harvested forest area over Europe after 2015. *Nature*, 583(7814), 72-77.

595 Ciais, P., A. J. Dolman, A. Bombelli, R. Duren, A. Peregon, P. J. Rayner, C. Miller, N. Gobron, G. Kinderman, G.
596 Marland, N. Gruber, F. Chevallier, R. J. Andres, G. Balsamo, L. Bopp, F.-M. Bréon, G. Broquet, R. Dargaville, T. J.
597 Battin, A. Borges, H. Bovensmann, M. Buchwitz, J. Butler, J. G. Canadell, R. B. Cook, R. DeFries, R. Engelen, K. R.
598 Gurney, C. Heinze, M. Heimann, A. Held, M. Henry, B. Law, S. Luysaert, J. Miller, T. Moriyama, C. Moulin, R. B.
599 Myneni, C. Nussli, M. Obersteiner, D. Ojima, Y. Pan, J.-D. Paris, S. L. Piao, B. Poulter, S. Plummer, S. Quegan, P.
600 Raymond, M. Reichstein, L. Rivier, C. Sabine, D. Schimel, O. Tarasova, R. Valentini, R. Wang, G. van der Werf, D.
601 Wickland, M. Williams, and C. Zehner (2014). "Current systematic carbon-cycle observations and the need for
602 implementing a policy-relevant carbon observing system". *Biogeosciences* 11.13, 3547–3602.

603 Chazdon, R. L., E. N. Broadbent, D. M. A. Rozendaal, F. Bongers, A. M. A. Zambrano, T. M. Aide, P. Balvanera, J. M.
604 Becknell, V. Boukili, P. H. S. Brancalion, D. Craven, J. S. Almeida-Cortez, G. A. L. Cabral, B. d. Jong, J. S. Denslow,
605 D. H. Dent, S. J. DeWalt, J. M. Dupuy, S. M. Durán, M. M. Espírito-Santo, M. C. Fandino, R. G. César, J. S. Hall, J. L.
606 Hernández-Stefanoni, C. C. Jakovac, A. B. Junqueira, D. Kennard, S. G. Letcher, M. Lohbeck, M. Martínez-Ramos, P.
607 Massoca, J. A. Meave, R. Mesquita, F. Mora, R. Muñoz, R. Muscarella, Y. R. F. Nunes, S. Ochoa-Gaona, E. Orihuela-
608 Belmonte, M. Peña-Claros, E. A. Pérez-García, D. Piotta, J. S. Powers, J. Rodríguez-Velazquez, I. E. Romero-Pérez, J.
609 Ruíz, J. G. Saldarriaga, A. Sanchez-Azofeifa, N. B. Schwartz, M. K. Steininger, N. G. Swenson, M. Uriarte, M. v.
610 Breugel, H. v. d. Wal, M. D. M. Veloso, H. Vester, I. C. G. Vieira, T. V. Bents, G. B. Williamson, and L. Poorter (2016).
611 "Carbon sequestration potential of second-growth forest regeneration in the Latin American tropics". *Science Advances*
612 2.5, e1501639.

613 Cook-Patton, S. C., Leavitt, S. M., Gibbs, D., Harris, N. L., Lister, K., Anderson-Teixeira, K. J., ... & Griscom, B. W.
614 (2020). Mapping carbon accumulation potential from global natural forest regrowth. *Nature*, 585(7826), 545-550.

615 Fick, S. E. and R. J. Hijmans (2017). "WorldClim 2: new 1-km spatial resolution climate surfaces for global land areas".
616 *International Journal of Climatology* 37.12, 4302–4315.

617 Hansen, M. C., P. V. Potapov, R. Moore, M. Hancher, S. A. Turubanova, A. Tyukavina, D. Thau, S. V. Stehman, S. J.
618 Goetz, T. R. Loveland, A. Kommareddy, A. Egorov, L. Chini, C. O. Justice, and J. R. G. Townshend (2013). "High-
619 Resolution Global Maps of 21st-Century Forest Cover Change". *Science* 342.6160, 850–853.

620 Huang, C., S. N. Goward, J. G. Masek, N. Thomas, Z. Zhu, and J. E. Vogelmann (2010). "An automated approach for
621 reconstructing recent forest disturbance history using dense Landsat time series stacks". *Remote Sensing of*
622 *Environment* 114.1, 183–198.

623 Giglio, L., L. Boschetti, D. P. Roy, M. L. Humber, and C. O. Justice (2018). "The Collection 6 MODIS burned area
624 mapping algorithm and product". *Remote Sensing of Environment* 217, 72–85.

625 Guyon, I., Weston, J., Barnhill, S., and Vapnik, V. (2002). "Gene selection for cancer classification using support vector
626 machines", *Mach. Learn.*, 46(1-3), 389–422.

627 Irvine, J., B. E. Law, and M. R. Kurpius (2005). "Coupling of canopy gas exchange with root and rhizosphere
628 respiration in a semi-arid forest". *Biogeochemistry* 73.1, 271–282.

629 Johnson, M. O., D. Galbraith, M. Gloor, H. D. Deurwaerder, M. Guimberteau, A. Rammig, K. Thonicke, H. Verbeeck,
630 C. v. Randow, A. Monteagudo, O. L. Phillips, R. J. W. Brienen, T. R. Feldpausch, G. L. Gonzalez, S. Fauset, C. A.
631 Quesada, B. Christoffersen, P. Ciais, G. Sampaio, B. Kruijt, P. Meir, P. Moorcroft, K. Zhang, E. Alvarez-Davila, A. A. d.
632 Oliveira, I. Amaral, A. Andrade, L. E. O. C. Aragao, A. Araujo-Murakami, E. J. M. M. Arets, L. Arroyo, G. A. Aymard,
633 C. Baraloto, J. Barroso, D. Bonal, R. Boot, J. Camargo, J. Chave, A. Cogollo, F. C. Valverde, A. C. L. d. Costa, A. D.
634 Fiore, L. Ferreira, N. Higuchi, E. N. Honorio, T. J. Killeen, S. G. Laurance, W. F. Laurance, J. Licona, T. Lovejoy, Y.
635 Malhi, B. Marimon, B. H. Marimon, D. C. L. Matos, C. Mendoza, D. A. Neill, G. Pardo, M. Peña-Claros, N. C. A.
636 Pitman, L. Poorter, A. Prieto, H. Ramirez-Angulo, A. Roopsind, A. Rudas, R. P. Salomao, M. Silveira, J. Stropp, H. t.
637 Steege, J. Terborgh, R. Thomas, M. Toledo, A. Torres-Lezama, G. M. F. v. d. Heijden, R. Vasquez, I. C. G. Vieira, E.
638 Vilanova, V. A. Vos, and T. R. Baker (2016). "Variation in stem mortality rates determines patterns of above-ground
639 biomass in Amazonian forests: implications for dynamic global vegetation models". *Global Change Biology* 22.12,
640 3996–4013.

641 Johnson, D. W. and P. S. Curtis (2001). "Effects of forest management on soil C and N storage: meta analysis". *Forest*
642 *Ecology and Management* 140.2, 227–238.

643 Jung, M., Schwalm, C., Migliavacca, M., Walther, S., Camps-Valls, G., Koirala, S., ... & Reichstein, M. (2020). Scaling
644 carbon fluxes from eddy covariance sites to globe: synthesis and evaluation of the FLUXCOM approach.
645 *Biogeosciences*, 17(5), 1343-1365.

646 Jung, M., M. Reichstein, H. A. Margolis, A. Cescatti, A. D. Richardson, M. A. Arain, A. Arneeth, C. Bernhofer, D. Bonal,
647 J. Chen, D. Gianelle, N. Gobron, G. Kiely, W. Kutsch, G. Lasslop, B. E. Law, A. Lindroth, L. Merbold, L. Montagnani,
648 E. J. Moors, D. Papale, M. Sottocornola, F. Vaccari, and C. Williams (2011). "Global patterns of land-atmosphere fluxes
649 of carbon dioxide, latent heat, and sensible heat derived from eddy covariance, satellite, and meteorological
650 observations". *Journal of Geophysical Research: Biogeosciences* 116.G3.

651 Kennedy, R. E., Z. Yang, and W. B. Cohen (2010). "Detecting trends in forest disturbance and recovery using yearly
652 Landsat time series: 1. LandTrendr — Temporal segmentation algorithms". *Remote Sensing of Environment* 114.12,
653 2897–2910.

654 Lewis, S. L., B. Sonké, T. Sunderland, S. K. Begne, G. Lopez-Gonzalez, G. M. F. van der Heijden, O. L. Phillips, K.
655 Affum-Baffoe, T. R. Baker, L. Banin, J.-F. Bastin, H. Beeckman, P. Boeckx, J. Bogaert, C. De Cannière, E. Chezeaux,
656 C. J. Clark, M. Collins, G. Djagbletey, M. N. K. Djuikouo, V. Droissart, J.-L. Doucet, C. E. N. Ewango, S. Fauset, T. R.
657 Feldpausch, E. G. Foli, J.-F. Gillet, A. C. Hamilton, D. J. Harris, T. B. Hart, T. de Haulleville, A. Hladik, K. Hufkens, D.
658 Huygens, P. Jeanmart, K. J. Jeffery, E. Kearsley, M. E. Leal, J. Lloyd, J. C. Lovett, J.-R. Makana, Y. Malhi, A. R.
659 Marshall, L. Ojo, K. S.-H. Peh, G. Pickavance, J. R. Poulsen, J. M. Reitsma, D. Sheil, M. Simo, K. Steppe, H. E.
660 Taedoumg, J. Talbot, J. R. D. Taplin, D. Taylor, S. C. Thomas, B. Toirambe, H. Verbeeck, J. Vleminckx, L. J. T. White,
661 S. Willcock, H. Woell, and L. Zomagho (2013). "Above-ground biomass and structure of 260 African tropical forests".
662 *Philosophical Transactions of the Royal Society B: Biological Sciences* 368.1625, 20120295.

663 Liu, S., B. Bond-Lamberty, J. A. Hicke, R. Vargas, S. Zhao, J. Chen, S. L. Edburg, Y. Hu, J. Liu, A. D. McGuire, J.
664 Xiao, R. Keane, W. Yuan, J. Tang, Y. Luo, C. Potter, and J. Oeding (2011). "Simulating the impacts of disturbances on
665 forest carbon cycling in North America: Processes, data, models, and challenges". *Journal of Geophysical Research:*
666 *Biogeosciences* 116.G4.

667 Lundberg, S. M., Erion, G. G., & Lee, S. I. (2018). Consistent individualized feature attribution for tree ensembles.
668 arXiv preprint arXiv:1802.03888.

669 Lundberg, S. M., & Lee, S. I. (2017). A unified approach to interpreting model predictions. In *Advances in neural
670 information processing systems* (pp. 4765-4774).

671 Mitchard, E. T. A., T. R. Feldpausch, R. J. W. Brienen, G. Lopez-Gonzalez, A. Monteagudo, T. R. Baker, S. L. Lewis, J.
672 Lloyd, C. A. Quesada, M. Gloor, H. t. Steege, P. Meir, E. Alvarez, A. Araujo-Murakami, L. E. O. C. Aragão, L. Arroyo,
673 G. Aymard, O. Banki, D. Bonal, S. Brown, F. I. Brown, C. E. Cerón, V. C. Moscoso, J. Chave, J. A. Comiskey, F.
674 Cornejo, M. C. Medina, L. D. Costa, F. R. C. Costa, A. D. Fiore, T. F. Domingues, T. L. Erwin, T. Frederickson, N.
675 Higuchi, E. N. H. Coronado, T. J. Killeen, W. F. Laurance, C. Levis, W. E. Magnusson, B. S. Marimon, B. H. M. Junior,
676 I. M. Polo, P. Mishra, M. T. Nascimento, D. Neill, M. P. N. Vargas, W. A. Palacios, A. Parada, G. P. Molina, M. Peña-
677 Claros, N. Pitman, C. A. Peres, L. Poorter, A. Prieto, H. Ramirez-Angulo, Z. R. Correa, A. Roopsind, K. H. Roucoux, A.
678 Rudas, R. P. Salomão, J. Schiatti, M. Silveira, P. F. d. Souza, M. K. Steininger, J. Stropp, J. Terborgh, R. Thomas, M.
679 Toledo, A. Torres-Lezama, T. R. v. Andel, G. M. F. v. d. Heijden, I. C. G. Vieira, S. Vieira, E. Vilanova-Torre, V. A. Vos,
680 O. Wang, C. E. Zartman, Y. Malhi, and O. L. Phillips (2014). “Markedly divergent estimates of Amazon forest carbon
681 density from ground plots and satellites”. *Global Ecology and Biogeography* 23.8, 935–946.

682 Moore, D. J. P., N. A. Trahan, P. Wilkes, T. Quaipe, B. B. Stephens, K. Elder, A. R. Desai, J. Negron, and R. K. Monson
683 (2013). “Persistent reduced ecosystem respiration after insect disturbance in high elevation forests”. *Ecology Letters*
684 16.6, 731–737.

685 N’Guessan, A. E., J. K. N’dja, O. N. Yao, B. H. K. Amani, R. G. Z. Gouli, C. Piponiot, I. C. Zo-Bi, and B. Hérault
686 (2019). “Drivers of biomass recovery in a secondary forested landscape of West Africa”. *Forest Ecology and*
687 *Management* 433, 325–331.

688 Naudts, K., Chen, Y., McGrath, M. J., Ryder, J., Valade, A., Otto, J., & Luyssaert, S. (2016). Europe’s forest
689 management did not mitigate climate warming. *Science*, 351(6273), 597-600.

690 Odum, E. P. (1969). “The Strategy of Ecosystem Development”. *Science* 164.3877, 262–270.

691 Pan, Y., J. M. Chen, R. Birdsey, K. McCullough, L. He, and F. Deng (2011). “Age structure and disturbance legacy of
692 North American forests”. *Biogeosciences* 8.3, 715–732.

693 Piponiot, C., Derroire, G., Descroix, L., Mazzei, L., Rutishauser, E., Sist, P., & Hérault, B. (2018). Assessing timber
694 volume recovery after disturbance in tropical forests—a new modelling framework. *Ecological Modelling*, 384, 353-369.

695 Ploton, P., Mortier, F., Réjou-Méchain, M., Barbier, N., Picard, N., Rossi, V., ... & Pélissier, R. (2020). Spatial validation
696 reveals poor predictive performance of large-scale ecological mapping models. *Nature communications*, 11 (1), 1-11.

697 Poorter, L., F. Bongers, T. M. Aide, A. M. Almeyda Zambrano, P. Balvanera, J. M. Becknell, V. Boukili, P. H. S.
698 Brancalion, E. N. Broadbent, R. L. Chazdon, D. Craven, J. S. de Almeida- Cortez, G. A. L. Cabral, B. H. J. de Jong, J.
699 S. Denslow, D. H. Dent, S. J. DeWalt, J. M. Dupuy, S. M. Durán, M. M. Espírito-Santo, M. C. Fandino, R. G. César, J.
700 S. Hall, J. L. Hernandez-Stefanoni, C. C. Jakovac, A. B. Junqueira, D. Kennard, S. G. Letcher, J.-C. Licona, M.
701 Lohbeck, E. Marín-Spiotta, M. Martínez-Ramos, P. Massoca, J. A. Meave, R. Mesquita, F. Mora, R. Muñoz, R.
702 Muscarella, Y. R. F. Nunes, S. Ochoa-Gaona, A. A. de Oliveira, E. Orihuela-Belmonte, M. Peña-Claros, E. A. Pérez-

703 García, D. Piotta, J. S. Powers, J. Rodríguez-Velázquez, I. E. Romero-Pérez, J. Ruíz, J. G. Saldarriaga, A. Sanchez-
704 Azofeifa, N. B. Schwartz, M. K. Steininger, N. G. Swenson, M. Toledo, M. Uriarte, M. van Breugel, H. van der Wal, M.
705 D. M. Veloso, H. F. M. Vester, A. Vicentini, I. C. G. Vieira, T. V. Bentos, G. B. Williamson, and D. M. A. Rozendaal
706 (2016). “Biomass resilience of Neotropical secondary forests”. *Nature* 530.7589, 211–214.

707 Poulter, B., L. Aragão, N. Andela, V. Bellassen, P. Ciais, T. Kato, X. Lin, B. Nachin, S. Luysaert, N. Pederson, P.
708 Peylin, S. Piao, T. Pugh, S. Saatchi, D. Schepaschenko, M. Schelhaas, and A. Shvidenko (2019). The global forest age
709 dataset and its uncertainties (GFADv1.1). PANGAEA- Data Publisher for Earth & Environmental Science.

710 Pugh, T. A. M., M. Lindeskog, B. Smith, B. Poulter, A. Arneeth, V. Haverd, and L. Calle (2019). “Role of forest regrowth
711 in global carbon sink dynamics”. *Proceedings of the National Academy of Sciences* 116.10, 4382–4387.

712 Schepaschenko, D., A. Shvidenko, V. Usoltsev, P. Lakyda, Y. Luo, R. Vasylyshyn, I. Lakyda, Y. Myklush, L. See, I.
713 McCallum, S. Fritz, F. Kraxner, and M. Obersteiner (2017). “A dataset of forest biomass structure for Eurasia”.
714 *Scientific Data* 4, 170070.

715 Schimel, D. (2007). “Carbon cycle conundrums”. *Proceedings of the National Academy of Sciences* 104.47, 18353–
716 18354.

717 Somogyi, Z., M. Teobaldelli, S. Federici, G. Matteucci, V. Pagliari, G. Grassi, and G. Seufert (2008). “Allometric
718 biomass and carbon factors database”. *iForest - Biogeosciences and Forestry* 1.3, 107.

719 Sulla-Menashe, D., C. E. Woodcock, and M. A. Friedl (2018). “Canadian boreal forest greening and browning trends:
720 an analysis of biogeographic patterns and the relative roles of disturbance versus climate drivers”. *Environmental*
721 *Research Letters* 13.1, 014007.

722 Sullivan, M. J. P., J. Talbot, S. L. Lewis, O. L. Phillips, L. Qie, S. K. Begne, J. Chave, A. Cuni-Sanchez, W. Hubau, G.
723 Lopez-Gonzalez, L. Miles, A. Monteagudo-Mendoza, B. Sonké, et al. (2017). “Diversity and carbon storage across the
724 tropical forest biome”. *Scientific Reports* 7, 39102

725 Tramontana, G., M. Jung, C. R. Schwalm, K. Ichii, G. Camps-Valls, B. Ráduly, M. Reichstein, M. A. Arain, A. Cescatti,
726 G. Kiely, L. Merbold, P. Serrano-Ortiz, S. Sickert, S. Wolf, and D. Papale (2016). “Predicting carbon dioxide and
727 energy fluxes across global FLUXNET sites with regression algorithms”. *Biogeosciences* 13.14, 4291–4313.

728 Werf, G. R. v. d., J. T. Randerson, L. Giglio, T. T. v. Leeuwen, Y. Chen, B. M. Rogers, M. Mu, M. J. E. v. Marle, D. C.
729 Morton, G. J. Collatz, R. J. Yokelson, and P. S. Kasibhatla (2017). “Global fire emissions estimates during 1997–2016”.
730 *Earth System Science Data* 9.2, 697–720.

731 Williams, C. A., G. J. Collatz, J. Masek, and S. N. Goward (2012). “Carbon consequences of forest disturbance and
732 recovery across the conterminous United States”. *Global Biogeochemical Cycles* 26.1.

733 Woodbury, P. B., J. E. Smith, and L. S. Heath (2007). “Carbon sequestration in the U.S. forest sector from 1990 to
734 2010”. *Forest Ecology and Management*. 241: 14-27. 241.

735 Zhu, Z., S. Piao, R. B. Myneni, M. Huang, Z. Zeng, J. G. Canadell, P. Ciais, S. Sitch, P. Friedlingstein, A. Arneeth, C.
736 Cao, L. Cheng, E. Kato, C. Koven, Y. Li, X. Lian, Y. Liu, R. Liu, J. Mao, Y. Pan, S. Peng, J. Peñuelas, B. Poulter, T. A.

- 737 M. Pugh, B. D. Stocker, N. Viovy, X. Wang, Y. Wang, Z. Xiao, H. Yang, S. Zaehle, and N. Zeng (2016). “Greening of
738 the Earth and its drivers”. *Nature Climate Change* 6.8, 791–795.
- 739 Zscheischler, J., M. D. Mahecha, V. Avitabile, L. Calle, N. Carvalhais, P. Ciais, F. Gans, N. Gruber, J. Hartmann, M.
740 Herold, K. Ichii, M. Jung, P. Landschützer, G. G. Laruelle, R. Lauerwald, D. Papale, P. Peylin, B. Poulter, D. Ray, P.
741 Regnier, C. Rödenbeck, R. M. Roman-Cuesta, C. Schwalm, G. Tramontana, A. Tyukavina, R. Valentini, G. v. d. Werf, T.
742 O. West, J. E. Wolf, and M. Reichstein (2017). “Reviews and syntheses: An empirical spatiotemporal description of the
743 global surface–atmosphere carbon fluxes: opportunities and data limitations”. *Biogeosciences* 14.15, 3685–3703.
- 744 Zhang, Y., Y. Yao, X. Wang, Y. Liu, and S. Piao (2017). “Mapping spatial distribution of forest age in China”. *Earth and
745 Space Science* 4.3, 108–116.